Atomic Force Microscopy Force-Distance Curves With Small Amplitude Ultrasonic Modulation

Chengfu Ma, Yuhang Chen, Tian Wang, and Jiaru Chu

Department of Precision Machinery and Precision Instrumentation, University of Science and Technology of China, Hefei, Anhui, P.R. China

Summary: Force-distance curves were acquired on a highly oriented pyrolytic graphite (HOPG) specimen and a gold film specimen under ultrasonic modulation in atomic force microscopy (AFM). Measurements demonstrated that small amplitude ultrasonic oscillation of either the cantilever or the sample has significant impacts on the characteristics of force-distance curves. With the increase of excitation amplitude, the apparent pull-off force decreased gradually and the hysteresis between the approach and retraction curves reduced significantly. Furthermore, the decrease of the pull-off force was determined to be also relevant to the excitation frequency. With the assistance of contact resonance spectra, the pull-off force was verified to have a near-linear relationship with the cantilever contact oscillation amplitude. Theoretical analysis and subsequent numerical simulations well interpreted the experimental results. The emergence of large oscillating contact forces under ultrasonic modulation altered the force-distance curves, and such a mechanism was ascertained by further ultrasonic AFM imaging. SCANNING 37:284–293, 2015. © 2015 Wiley Periodicals, Inc.

Key words: atomic force microscopy, force-distance curves, ultrasonic modulation, pull-off force, force spectroscopy

Introduction

Since its invention, atomic force microscopy (AFM) has emerged as a powerful tool in many fields of nanoscience and nanotechnology. As one of the most basic operations of almost all AFM instruments, force spectroscopy or more technically the force-distance curves method (Cappella and Dietler, '99) is of fundamental importance. In measurements of force-distance curves, the cantilever deflection is acquired as a function of displacement by approaching and retracting the tip from the sample surface. With precise calibration of the spring constant of the cantilever, various types of interaction forces are able to be revealed. Force-distance curves method has been routinely employed to characterize van der Waals, capillary, hydration, electrostatic, single-molecule interaction forces, etc. (Weisenhorn et al., '89; Butt, '91; Eastman and Zhu, '96; Strunz et al.,'99).

In general, force-distance curves acquired in ambient air have some common characteristics such as a sudden jump-to-contact when approaching the tip and a jump-off-contact when retracting. The jump-to-contact is originally caused by instability of the effective tip-sample potential at distance where the force gradient of the tip-sample interaction becomes larger than the spring constant of the cantilever (Cappella and Dietler, '99). The jump-off-contact is commonly interpreted as the presence of adhesion forces (Zlatanova et al., 2000). The coexistence of jump-to-contact and jump-off-contact gives rise to discontinuities and hysteresis of the force-distance curves. Force-distance curves obtained in liquid environment can eliminate the hysteresis where meniscus forces caused by thin water layers absorbed on the surface are dramatically reduced (Weisenhorn et al., '89). In such a way, small tip-sample contact forces can be maintained in raster scan, which can be beneficial for imaging soft materials with relatively gentle indentations. Besides applications in exploring tip-sample interactions, force-distance curves are also important for the proper selection of imaging

parameters and the calibration of optical lever sensitivity.

Conventional force-distance curves are usually acquired in a quasi-static manner. However, we should note that various dynamic imaging modes have already been developed where static force-distance curves are not enough for characterizations of tip-sample interactions and the cantilever responses. In particular, AFMs combined with ultrasonic vibration have obtained great applications in material properties measurement (Yamanaka *et al.*, '99; Hurley *et al.*, 2005; Huey, 2007), subsurface imaging (Yamanaka *et al.*, '94; Shekhawat and Dravid, 2005; Tetard *et al.*, 2010), and nano-machining (Zhang and Dong, 2012) in recent years. Among them, atomic force acoustic microscopy (AFAM) and ultrasonic atomic force microscopy (UAFM) have achieved great successes in characterizing elastic properties quantitatively and visualizing subsurface features to a depth of several hundreds of nanometers (Rabe *et al.*, 2000; Tsuji *et al.*, 2002; Hurley *et al.*, 2006; Striegler *et al.*, 2011; Kimura *et al.*, 2013). However, the complexities of cantilever dynamics and tip-sample interactions in these operation modes make the precise data interpretation quite difficult.

Until now, how the ultrasonic excitation affects the tip-sample interactions and the cantilever dynamics has not been fully understood, though there have already been some investigations from the aspects of resonance spectra (Rabe *et al.*, '99; Rabe *et al.*, 2002) or force-distance curves (Matsuda *et al.*, 2002) independently. For a more comprehensive study, we combined force-distance curves with ultrasonic modulations in this work. First, the influences of excitation amplitude and frequency on force-distance curves were investigated experimentally. Second, we verified the experimental results and corresponding model interpretations by numerical simulations. Finally, we performed UAFM imaging on a gold film specimen and a highly oriented pyrolytic graphite (HOPG) specimen to provide a complementary elucidation of the role of modulation in tip-sample interactions.

Materials and Methods

Experimental

The experiments were performed on a homemade contact resonance (CR) AFM platform (Yang *et al.*, 2013) as schematically illustrated in Figure 1, which was realized by modifying a commercial AFM (Nanotec Electrónica, Madrid, Spain). Both UAFM and AFAM could be employed, and the results demonstrated here were performed in the UAFM mode if not specifically pointed out. The signal generator module of a computer-controlled digital lock-in amplifier HF2LI (Zurich Instruments, Zurich, Switzerland) was used to provide
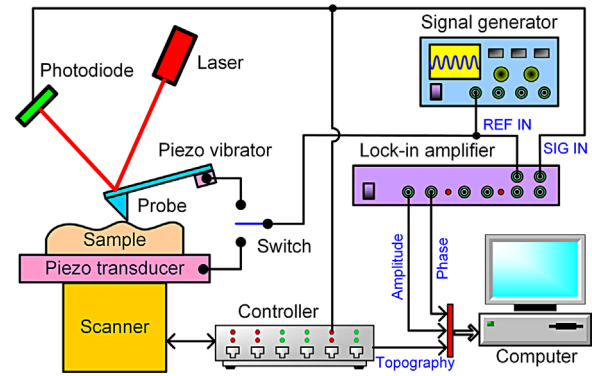

Fig. 1.   Schematic illustration of the CR-mode AFM. Both UAFM (cantilever excitation) and AFAM (sample excitation) can be easily realized via a switch.

high-frequency excitation signals to drive the cantilever via a shaker-piezo. The cantilever deflection was detected by a position-sensitive detector (PSD) and then fed into the lock-in amplifier. Then the amplitude and phase were extracted and imported subsequently into WSxM software (Horcas *et al.*, 2007) for data acquisition and post-processing, together with other signal channels such as topography, normal force and lateral force.

Two samples with different stiffness and adhesion properties were used, namely a gold film specimen and a HOPG specimen. The former has considerably larger adhesion properties than the latter. The gold film was prepared by sputtering deposition. One layer of 10 nm thick titanium was first sputtered onto a silicon substrate using a SP-2 type magnetron sputtering station (Institute of Microelectronics of Chinese Academy of Sciences, Beijing, China) to strengthen the bonding to the substrate. Then one layer of 50 nm thick gold was subsequently sputtered onto the titanium film. The HOPG specimen was freshly cleaved before measurements. The cantilever used in the experiments was a ContAl-G cantilever (Budget Sensors, Sofia, Bulgaria). The first three free resonant frequencies in air were determined to be 13.3, 85.1, and 239.5 kHz, respectively, and the spring constant $k_c = 0.27$ N/m by thermal calibration (Hutter and Bechhoefer, '93).

Three different types of experiments were carried out. The first one is the determination of the CR frequencies. The tip was brought into contact with the sample surface, and then a frequency-sweeping excitation was added to the shaker-piezo. The cantilever oscillation was analyzed by the lock-in amplifier and the amplitude and phase spectra were obtained subsequently. From the amplitude spectrum, the CR frequencies can be easily determined as well as the actual cantilever contact oscillation amplitude at each driven frequency. The second type is the acquisition of force-distance curves (see Fig. 3). The force-distance curves were measured by first

withdrawing and then approaching the tip from the sample surface while vibrating the cantilever at ultrasonic frequency. A series of force-distance measurements with different excitation amplitudes and frequencies were implemented. The third experiment is the UAFM imaging (see Figs. 9 and 10). The topography, normal force, and lateral force channels were mainly analyzed for a complementary verification of the proposed theoretical interpretations and numerical simulations. The influence of ultrasonic modulation on these signals was additionally discussed.

Numerical Simulation

To provide a comprehensive understanding of the real-time tip-sample interactions, numerical calculations were performed. A simplified AFM system model was adopted. It contains the cantilever dynamics module, the tip-sample interaction forces module, the distance sweep module and the ultrasonic modulation module. The flow diagram is schematically shown in Figure 2. The distance sweep applies approaching/retracting displacements of the cantilever and the ultrasonic modulation introduces additional variations of the tip-sample gap. The computations were performed during the distance sweep at a constant rate until the entire force-distance curves were traversed. At each location, the real-time cantilever deflection and interaction forces were calculated. The deflection was determined by comparing the tip position and the swept cantilever base position. Finally, the real-time deflection and interaction forces as functions of tip displacement and ultrasonic excitation parameters were obtained and exported for further analysis.

The Derjaguin–Müller–Toporov (DMT) model (Derjaguin et al., '75) was used to describe the tip-sample interaction forces. The DMT model combines noncontact van der Waals forces with Hertz contact forces, and is valid for low adhesive, stiff contacts in vacuum or air. For a tip-sample gap d, the force model can be written as,

$$F_{ts}(d) = \begin{cases} -\dfrac{HR}{6d^2}, & d > a_0 \\ -\dfrac{HR}{6a_0^2} + \dfrac{4}{3}E^*\sqrt{R}(a_0 - d)^{3/2}, & d \leq a_0 \end{cases}$$
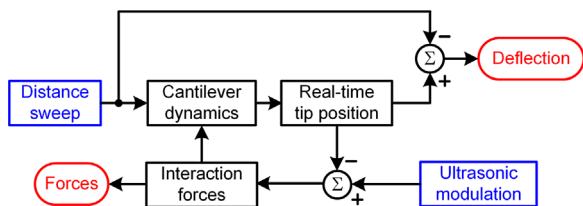
(1)

Fig. 2. Flow diagram of the simplified model for simulating force-distance curves under ultrasonic excitation.

where a_0 is the intermolecular distance, and $d = a_0$ denotes the sample surface. H is the Hamaker constant and R is the tip radius. $E^* = \left(\dfrac{1-\nu_{tip}^2}{E_{tip}} + \dfrac{1-\nu_{sample}^2}{E_{sample}}\right)^{-1}$ is the reduced elastic modulus of the tip and sample, in which E and ν are the elastic modulus and Poisson's ratio, and the subscripts *tip* and *sample* mean that values are defined for the tip and sample, respectively.

The cantilever dynamics was modeled by a one-degree-of-freedom system. The system is equivalent to a mass m and spring constant k and damping coefficient γ. Such a model has been verified to be appropriate in dynamic AFM in air despite its simplification (Rodŕguez and Garća, 2002). Considering the tip-sample interaction forces F_{ts} and the driving force F_{driven}, the second-order differential equation of the cantilever motion can be described as,

$$m\dot{z} + \gamma z + kz = F_{driven} + F_{ts}$$

(2)

Here, the damping is characterized by quality factor Q as $\gamma = m\omega_0/Q$, in which $\omega_0 = 2\pi f_0$ is the natural angular frequency of the cantilever and f_0 is the natural frequency. It should be mentioned that the ultrasonic excitation is given in the form of tip-sample distance modulation. Thus, the driving force F_{driven} in our simulations is replaced by a distance modulation $A_d\cos(\omega_d t)$, where A_d and $\omega_d = 2\pi f_d$ are, respectively, the excitation amplitude and angular frequency, and f_d is the excitation frequency. The ultrasonic modulation changes the cantilever dynamics only when the tip is close to or in contact with the sample surface. Equation 2 can be numerically solved by using conventional fourth-order Runge–Kutta algorithm.

Results and Discussion

Force-Distance Curves With Ultrasonic Modulation

Force-distance curves measurements were performed on the HOPG specimen by applying ultrasonic excitations to the cantilever with different amplitudes, namely in UAFM mode. Prior to that, a frequency sweep was done while the tip contacting the sample surface at a static load of 108 nN. As a result, the first CR frequency was determined to be 64.3 kHz. Then excitations with frequency of 64.0 kHz and various amplitudes up to 5 V were exerted on the shaker-piezo during force-distance curves measurements. Typical results are presented in Figure 3. In the case of no ultrasonic modulation, the curves are exactly the typical ones measured in ambient air. There are a large jump-off-contact around the location of 231 nm in the retraction curve (blue) and a small but distinguishable jump-to-contact around 623 nm in the approach curve (red). With
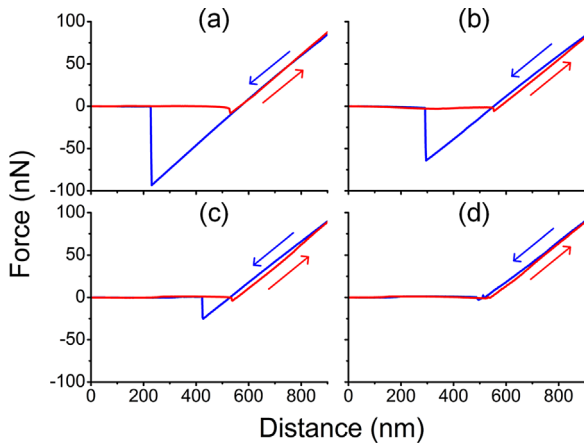
Fig. 3.   Force-distance curves on HOPG with different ultrasonic excitation amplitudes but the same frequency. The excitation amplitudes are, respectively: (a) no vibration; (b) 1 V; (c) 2 V; (d) 3 V. The arrows illustrate the approaching (red) and withdrawing (blue) directions.

increasing the excitation amplitude, the jump-off position gradually moves closer to the jump-in position while the latter remains almost unchanged. Correspondingly, the apparent pull-off force decreases monotonously. At larger amplitude of 3 V, both the jump-to-contact and jump-off-contact disappear, and the hysteresis between the approach and retraction curves is eliminated. Such features are actually quite similar to those obtained in liquid environments.

Moreover, same experiments in AFAM mode, that is, applying the excitation to the sample instead of the cantilever, have been additionally carried out. The results are in fact identical to the ones in UAFM but only with certain noisy spikes in the contact regions of the force-distance curves especially when relatively large excitation amplitudes are employed.

For a quantitative evaluation of the influence of excitation amplitude on force-distance curves, characteristic parameters were extracted and compared. Figure 4 shows the pull-off forces and pull-off distances under different excitation amplitudes. It can be found that both of them decrease monotonously with increasing the excitation amplitude. The trends indicate a strong influence of the ultrasonic excitation on the acquired force-distance characteristics.

Impact of Contact Dynamics

From above preliminary results, the reduction of the apparent pull-off force is supposed to have a close relationship with the cantilever dynamic responses, which are relevant to both excitation amplitude and frequency. So, how the actual cantilever vibration alter the force-distance curves? To answer this question,

systematic measurements of force-distance curves on the gold film specimen were performed. The first series of experiments are toward the purpose of examining the influence of cantilever contact amplitude. In measurements, the excitation frequency was chosen to be 65.8 kHz, near the first CR frequency at a preload of 73 nN. Figure 5(a) shows the extracted pull-off forces. Behaviors that are similar to the ones on the HOPG specimen were observed. It is well known that the cantilever contact dynamics will gradually exhibit evident nonlinearity while increasing the excitation amplitude (Rabe *et al.*, '99; Rabe *et al.*, 2002). That is, the actual cantilever contact amplitude will not be in a simple linear relationship with the excitation amplitude. Therefore, to establish the link between the pull-off force and the cantilever contact amplitude, CR amplitude spectra were acquired before each force-curves measurement. Figure 5(b) presents contact amplitudes at the chosen frequency while altering the excitation amplitude. An evident nonlinearity can be observed, especially under relatively large excitation amplitudes like 4.5 V and 5 V. At such excitation amplitudes, the resonance peaks shift to the left-hand side corresponding to a so-called softening non-linearity (Muraoka and Arnold, 2001), and the cantilever amplitudes at the chosen frequencies decrease conversely. Figure 5(c) demonstrates pull-off forces taking cantilever contact amplitude as the abscissa. A near linear relation exists between the two parameters, and the slope is determined to be $-312k_c$ N/m by applying a least-square fit. The pull-off force decreases 8.4 nN per 100 pm increment of the contact amplitude.

Same investigations were applied around the second CR frequency. The results are listed in Figure 5(d–f). A linear relationship between the pull-off force and the cantilever contact amplitude was again obtained, though the relation between the pull-off force and the excitation amplitude behave much differently from the one around the first CR frequency. It should be noted that there are a few points with relatively small contact amplitudes where the pull-off forces are almost unchanged, which is most likely caused by measurement uncertainties since the contact amplitude nearly reaches the noise floor. For contact amplitude larger than about 100 pm, the pull-off force decreases linearly in a slope of $-3560k_c$ N/m with increasing the cantilever contact amplitude. The decrement of the pull-off force is almost 11.4 times faster compared with the ones around the first CR frequency. This kind of magnification is thought to be associated with the dynamic stiffening of the cantilever under higher vibration modes (Huey, 2007).

Subsequently, additional measurements under different excitation frequencies were applied to further study the influence of cantilever contact dynamics. A CR amplitude spectrum on the gold film specimen around the second CR frequency, as shown in Figure 6(a), was first swept with excitation amplitude of 5 V and a static
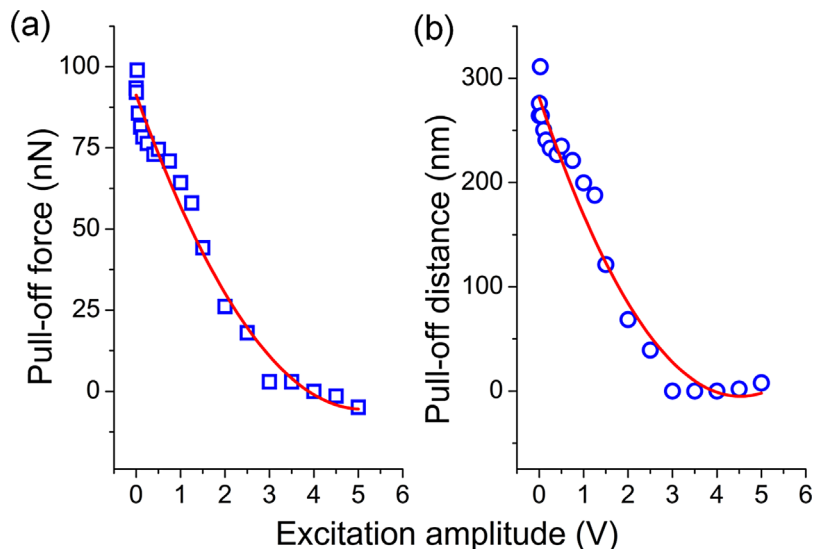
Fig. 4.   Characteristic parameters of force-distance curves under various excitation amplitudes. (a) Pull-off force. (b) Pull-off distance.

load of 73 nN. It can be found that the spectrum exists obvious non-linearity under such a large amplitude. Then, excitations with various different frequencies ranging over 200–250 kHz were exerted on the cantilever and force-distance curves were measured with other conditions unchanged. The pull-off forces under these frequencies were extracted and demonstrated in Figure 6(b). The variation tendency depicted in Figure 6 (b) is quite consistent in the shape with that part of the

spectrum in Figure 6(a) ranging over 200–250 kHz if we mirror the data against the horizontal axis. This is further verified when the relationship between the pull-off force and the cantilever contact amplitude are constructed, as can be seen in Figure 6(c). A near linear relation between them is obtained once again. However, the frequency-difference-induced effects are not reflected owing to the very limited frequency range here. With the assistance of contact resonance spectra, all the above
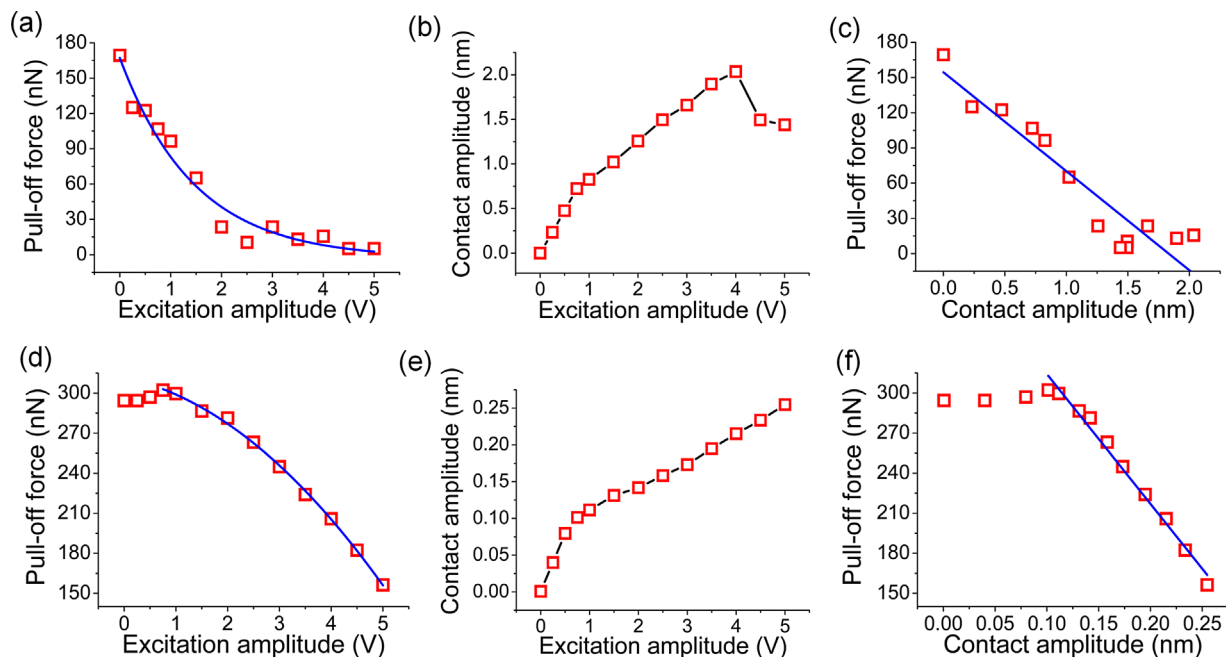

Fig. 5.   Influence of cantilever contact dynamics on the force-distance curves with different ultrasonic modulation amplitudes but the same excitation frequency. The results in the upper row are acquired around the first CR frequency and the ones in the lower row are obtained around the second CR frequency. (a) and (d): Pull-off forces under different excitation amplitudes. (b) and (e): Measured cantilever contact amplitudes under corresponding excitation amplitudes. (c) and (f): Dependence of the pull-off forces on the cantilever contact amplitudes.
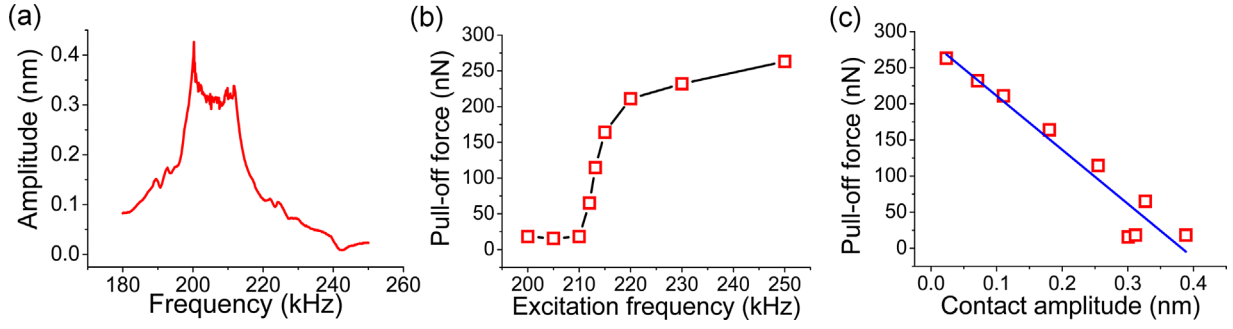
Fig. 6.   Influence of cantilever contact dynamics on the force-distance curves with different ultrasonic modulation frequencies but the same excitation amplitude. (a) Measured CR spectra. (b) Pull-off forces under different excitation frequencies. (c) Constructed relationship between the pull-off force and the cantilever contact amplitude.

experimental results demonstrated that the pull-off force decreases almost linearly with increasing the cantilever contact amplitude, though it has a complex nonlinear dependence on excitation amplitude and frequency.

Model Interpretation and Simulation Results

To study the mechanism behind the phenomena described in above sections, theoretical explanations and subsequent computations were employed. We start with a simple but intuitive explanation. A schematic illustration is depicted in Figure 7. The curve $F(D)$ represents the tip-sample interaction and the dotted lines 1, 2, and 3 denote the elastic restoring forces of the cantilever. In conventional static force-distance measurements, a jump-to-contact and a jump-off-contact will emerge at point α in the approach curve and at point β in the retraction curve owing to the instability of the effective tip-sample potential. However, if an ultrasonic modulation is applied, a small distance modulation $A(t)$ in the contact region will cause

a relatively large interaction modulation $F(t)$ because of the large force gradient. And at point b while retracting, the peak force of the interaction modulation $F(t)$ exceeds the minimum force in the interaction curve (point c). The jump-off-contact consequently occurs in advance and the jump-off point shifts to point B from point C. Therefore, the pull-off point moves a distance of $|\gamma\beta|$, and the pull-off force decreases with an amount of $|f_c f_b|$.

Considering the simplified tip-sample interaction model (see Equation 1), we derive the contact forces under ultrasonic excitation as,

$$F_{contact} = -\frac{HR}{6a_0^2} + \frac{4}{3}E^*\sqrt{R}[\delta_0 + \delta_A\cos(\omega_d t)]^{3/2} \quad (3)$$

where $\delta_0 = a_0 - d$ denotes the mean indentation depth. δ_A is the excitation-induced modulation amplitude of the indentation, which approximately equals the measured cantilever contact amplitude in experiment. With small amplitude assumption $\delta_A \approx 0$ and performing a Taylor expansion, the shift of the apparent pull-off force is finally estimated as,

$$\Delta F_{pull-off} = 2\sqrt{R\delta_0}E^*\delta_A \quad (4)$$

From which, we can find that $\Delta F_{pull-off} \propto \delta_A$, indicating an approximate linear dependence between the reduction of pull-off force and the cantilever contact amplitude. This is in accord with what we observed in the experiments, for instance Figure 5(c and f).

To ascertain the theoretical model, numerical simulations were applied by solving Equation 2. The cantilever parameters were set as spring constant $k_c = 0.5$ N/m, free resonance frequency $f_0 = 30$ kHz, and quality factor $Q = 50$. A silicon tip and a HOPG specimen were assumed. The tip radius R was set to be 10 nm, and the Hamaker constant $H = 3.5 \times 10^{-19}$ J, the intermolecular distance $a_0 = 0.4$ nm. A tip-sample distance of 16 nm was assigned as the start point, and then the approach process was simulated point by
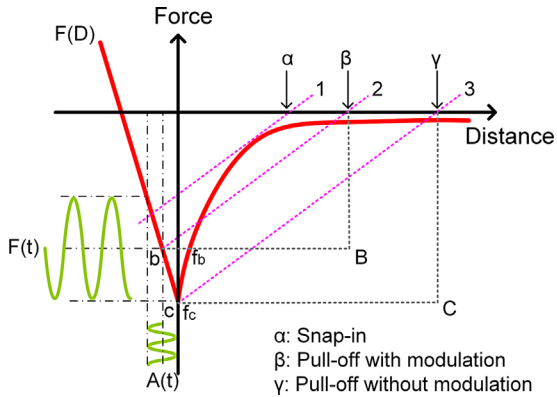

Fig. 7.   Illustration of the influence of ultrasonic modulation on the determined pull-off force. The solid curve $F(D)$ represents the tip-sample interaction forces and the dotted lines 1, 2, and 3 denote the elastic forces of the cantilever. The sinusoidal curve $A(t)$ represents the modulated tip vibration at point b, and $F(t)$ is the corresponding modulation-induced contact force oscillation.

point successively until an end location of $-2\,nm$ was reached. The retraction process was then carried out in the same manner until the start point. The approaching/withdrawing rate was set to be 216.0 nm/s and the total simulation time for a distance sweep of 18 nm was approximately 83.3 ms. For both curves, a time interval of $0.52\,\mu s$ was chosen, which is sufficiently small. Finally, the force-time curves were converted into force-distance curves and subsequently analyzed.

We applied a series of computations under different oscillation frequencies and amplitudes. The pull-off forces were extracted and plotted in a contour map as shown in Figure 8(a). It can be seen that both the oscillation frequency and amplitude affect the pull-off force significantly, which decreases evidently with increasing both of them. Picking out the pull-off forces under various oscillation amplitudes but a fixed frequency such as 40, 80, and 120 kHz, we can clearly find the influences of the two factors, which are demonstrated in Figure 8(b). A near linear relationship between the pull-off force and the oscillation amplitude presents. Moreover, it can be found that the pull-off force decreases more rapidly under higher excitation frequencies from the comparison of the three datasets. Therefore, the simulation results coincide quite well with what we observed in experiments (Figs. 4 and 5).

The main features are reasonably sketched in the simulations though the model actually neglects large adhesive interactions and complex dynamics of a cantilever beam.

Figure 8(c) shows two force-time curves under oscillation amplitudes of 0 and 30 pm, respectively. From both of the curves, the jump-to-contact and jump-off-contact can be distinguished. Compared with the no vibration case, the jump-in is almost unchanged in the 30 pm oscillation case. However, the jump-off happens in advance in the time which corresponds to an approach of the jump-off position to the jump-in position in distance, and the pull-off force decreases evidently. These simulation results are in good accordance with what we observed in the experiments (see Fig. 3). In addition, a relatively large oscillation of the interaction force in the contact region can be found unambiguously. And as long as the oscillating interaction force exceeds a critical threshold, the jump-off-contact happens. These confirm the theoretical explanation performed in Figure 7.

Imaging Verification

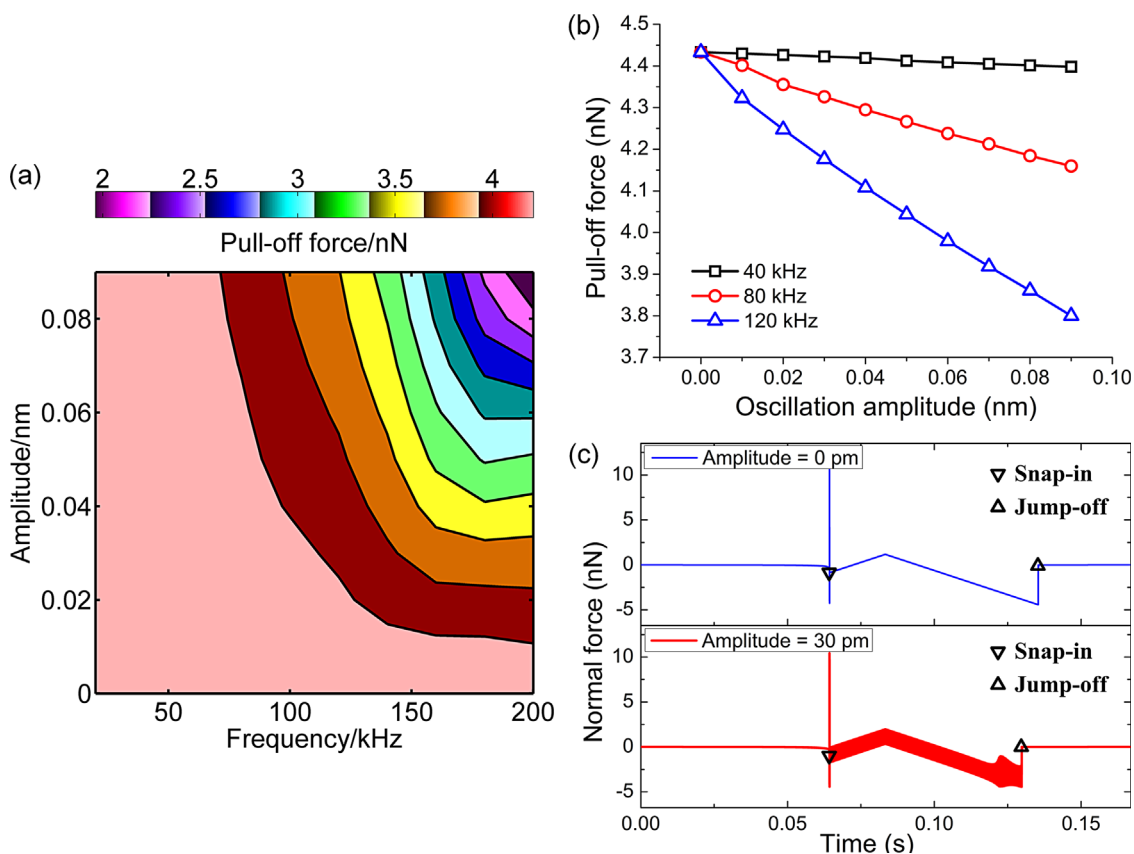UAFM imaging on the gold film specimen and the HOPG specimen was performed with different

Fig. 8.   Numerical simulation results of force-distance curves under ultrasonic modulation. (a) Contour map of the pull-off force as a function of the modulation amplitude and frequency. (b) Dependence of the pull-off force on the modulation amplitude at frequencies of 40, 80, and 120 kHz. (c) Force-time curves with modulation amplitudes of 0 and 30 pm.

excitation amplitudes in order to provide a complementary evidence of the influence of ultrasonic modulation. An area of $2 \times 2\,\mu m$ was scanned in 256×256 pixels on the gold film specimen with the excitation amplitude set to be 0, 0.05, 0.15, and 0.25 V, respectively. A relatively small set-point of 0.12 V was applied with a corresponding zero-force line of 0.10 V, and so the applied contact force was approximately 5.2 nN. The images were acquired with a scan rate of 2 Hz. The topography images are shown in Figure 9. We can find that the same area was scanned under different ultrasonic excitations imaging. However, permanent damages of the gold film occurred, one of which is marked by dashed circles. Since we actually set a small "apparent" contact force in scanning, serious damages are not expected. Therefore, the only explanation is that oscillating normal forces with large peak forces are actually applied on the sample surface though the average normal force remains small under the feedback control. For such soft materials, the oscillating indentation forces damage the specimen.

The UAFM imaging results on the HOPG specimen are presented in Figure 10. Here the scan size was 256×256 pixels for a $3 \times 3\,\mu m$ area, and the scan rate was 2 Hz. Excitation amplitudes of 0, 0.05, 0.15, 0.25, 0.75, and 1 V were employed. The zero-force line was at -0.06 V, and a small set-point of -0.02 V was applied, corresponding to 10.4 nN. Figure 10(a–c), respectively, show the topography, normal force and lateral force signals without ultrasonic modulation. And Figure 10 (d–f) show the ones for the excitation amplitude of 0.25 V. Comparing the images acquired under different excitation amplitudes, no evident visual differences are observable. However, when we perform some statistical analyses for the whole scan size, interesting results are obtained. Figure 10(g) shows the mean values and their standard deviations of normal forces. The mean values are almost unchanged since normal force is chosen as the feedback signal, but the standard deviations obviously decrease with increasing the excitation amplitudes, as shown in Figure 10(h). With small amplitude ultrasonic excitation, the influence of adhesion forces on the force-distance curves is
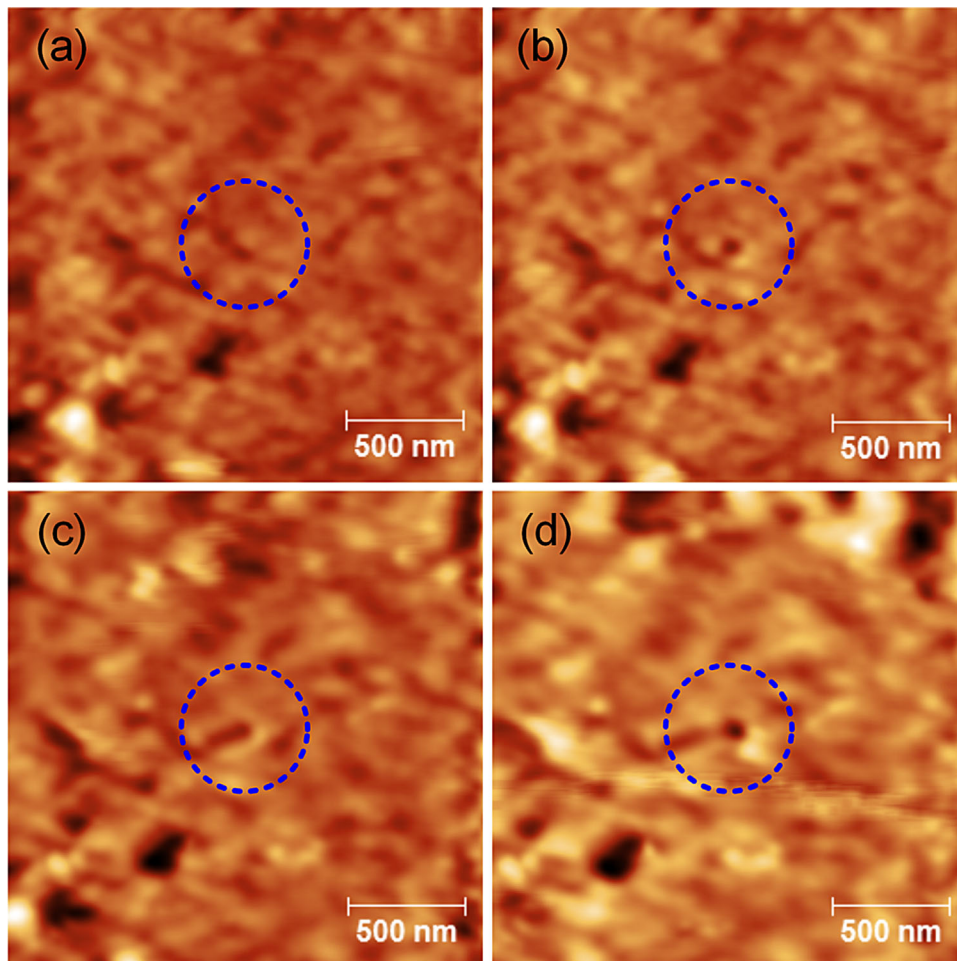

Fig. 9.   Topography images on the gold film under different ultrasonic excitation amplitudes. The excitation amplitudes are, respectively: (a) no vibration; (b) 0.05 V; (c) 0.15 V; (d) 0.25 V. The dashed circles show a gradually expanding damage area of the sample surface.
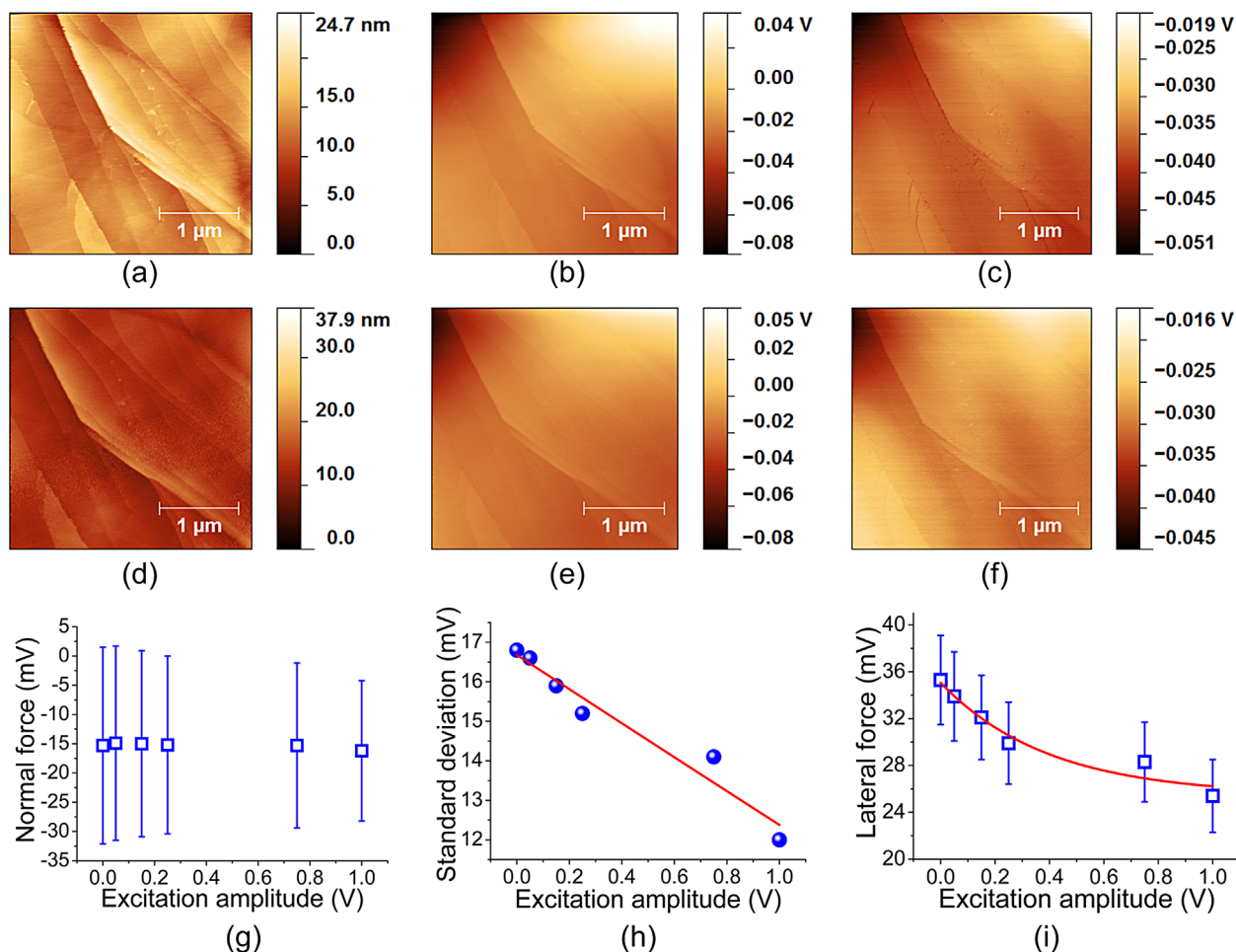
Fig. 10.   Imaging results with ultrasonic excitation on the HOPG specimen. (a–c) Topography, normal force and lateral force images without excitation. (d–f) Topography, normal force and lateral force images with excitation amplitude of 0.25 V. (g) Averaged normal forces, (h) standard deviations of normal forces, and (i) averaged lateral forces resulted from statistical analysis across the whole scan area, that is $3 \times 3\,\mu m$, under various excitation amplitudes.

eliminated (e.g. Fig. 3(d)). The normal force control therefore becomes much more stable because the effects of adhesion forces fluctuations become negligible in presence of appropriate ultrasonic modulation.

Same statistics of the lateral force images are shown in Figure 10(i), from which a gradual decrease of the lateral force can be found with increasing the excitation amplitude, suggesting the ultrasonic-oscillation-induced lubrication of the tip-sample contact. Better feedback force control and obvious elimination of frictional force indicate possible more stable imaging with respect to the traditional contact mode. Unfortunately, such advantages cannot lead to better topography imaging of soft samples as demonstrated in the measurements of gold film.

Conclusions

Force-distance curves measurements under small amplitude ultrasonic modulation were performed on a HOPG specimen and a gold film specimen. The force-distance curves, especially the retraction curve, changed evidently when altering the excitation amplitude and frequency. With increasing the excitation amplitude, the pull-off force gradually decreased. By measuring CR spectra, the pull-off force was finally verified to be in a near linear relationship with the cantilever contact amplitude. Moreover, it was found that the pull-off force decreased more rapidly under higher excitation frequencies.

The decrease of the pull-off force while increasing the cantilever contact amplitude and the near linear relationship between them were theoretically explained based on analyzing the force-distance curve and the tip-sample interactions. Subsequent simulations of the real-time force-distance curves demonstrated the interaction oscillation in the contact region intuitively. The shift of the pull-off distance and the decrease of the pull-off force under ultrasonic modulation were reasonably simulated. Further systematic simulations along with different excitation amplitudes and frequencies showed

that the pull-off force is in an, approximately, linear relationship with the cantilever amplitude and the corresponding slope is larger for higher excitation frequencies. These results coincide very well with the experimental ones.

UAFM imaging under various excitation amplitudes on the gold film specimen and HOPG specimen were also performed with a small set-point of the normal force. Sample damages were unambiguously distinguished on the gold film and these observations verified the existence of large oscillating contact force. The images on the HOPG specimen were analyzed quantitatively. The standard deviation of the normal force was found to decrease in a near linear manner with increasing the excitation amplitude. Such results indicate a more stable feedback force control in UAFM imaging. In addition, the average lateral forces were also decreased significantly, which can be associated with ultrasonic lubrication.

References

Butt H. 1991. Measuring electrostatic, van der Waals, and hydration forces in electrolyte solutions with an atomic force microscope. Biophys J 60:1438–1444.

Cappella B, Dietler G. 1999. Force-distance curves by atomic force microscopy. Surf Sci Rep 34:1–104.

Derjaguin BV, Muller VM, Toporov YP. 1975. Effect of contact deformations on the adhesion of particles. J Colloid Interf Sci 53:314–326.

Eastman T, Zhu DM. 1996. Adhesion forces between surface-modified AFM tips and a mica surface. Langmuir 12:2859–2862.

Horcas I, Fernandez R, Gomez-Rodriguez JM, et al. 2007. WSXM: A software for scanning probe microscopy and a tool for nanotechnology. Rev Sci Instrum 78:013705.

Huey BD. 2007. AFM and acoustics: Fast, quantitative nanomechanical mapping. Annu Rev Mater Res 37:351–385.

Hurley DC, Kopycinska-Muller M, Langlois ED, Kos AB, Barbosa N. 2006. Mapping substrate/film adhesion with contact-resonance-frequency atomic force microscopy. Appl Phys Lett 89:021911.

Hurley DC, Kopycinska-Müller M, Kos AB, Geiss RH. 2005. Nanoscale elastic-property measurements and mapping using atomic force acoustic microscopy methods. Meas Sci Technol 16:2167–2172.

Hutter JL, Bechhoefer J. 1993. Calibration of atomic-force microscope tips. Rev Sci Instrum 64:1868–1873.

Kimura K, Kobayashi K, Matsushige K, Yamada H. 2013. Imaging of Au nanoparticles deeply buried in polymer matrix by various atomic force microscopy techniques. Ultramicroscopy 133:41–49.

Matsuda O, Terada T, Inagaki K, Wright OB. 2002. Cantilever dynamics in ultrasonic force microscopy. Jpn J Appl Phys 41:3545–3546.

Muraoka M, Arnold W. 2001. A method of evaluating local elasticity and adhesion energy from the nonlinear response of AFM cantilever vibrations. JSME Int J A 44:396–405.

Rabe U, Amelio S, Kester E, et al. 2000. Quantitative determination of contact stiffness using atomic force acoustic microscopy. Ultrasonics 38:430–437.

Rabe U, Kester E, Arnold W. 1999. Probing linear and non-linear tip-sample interaction forces by atomic force acoustic microscopy. Surf Interface Anal 27:386–391.

Rabe U, Kopycinska M, Hirsekorn S, Arnold W. 2002. Evaluation of the contact resonance frequencies in atomic force microscopy as a method for surface characterisation. Ultrasonics 40:49–54.

Rodŕguez TR, Garća R. 2002. Tip motion in amplitude modulation (tapping-mode) atomic-force microscopy: Comparison between continuous and point-mass models. Appl Phys Lett 80:1646–1648.

Shekhawat GS, Dravid VP. 2005. Nanoscale imaging of buried structures via scanning near-field ultrasound holography. Science 310:89–92.

Striegler A, Koehler B, Bendjus B, et al. 2011. Detection of buried reference structures by use of atomic force acoustic microscopy. Ultramicroscopy 111:1405–1416.

Strunz T, Oroszlan K, Schafer R, Guntherodt HJ. 1999. Dynamic force spectroscopy of single DNA molecules. PNAS 961:11277–11282.

Tetard L, Passian A, Farahi RH, Thundat T. 2010. Atomic force microscopy of silica nanoparticles and carbon nanohorns in macrophages and red blood cells. Ultramicroscopy 110:586–591.

Tsuji T, Irihama H, Yamanaka K. 2002. Observation of anomalous dislocation behavior in graphite using ultrasonic atomic force microscopy. Jpn J Appl Phys 41:832–835.

Weisenhorn AL, Hansma PK, Albrecht TR, Quate CF. 1989. Forces in atomic force microscopy in air and water. Appl Phys Lett 54:2651–2653.

Yang C, Chen Y, Wang T, Huang W. 2013. A comparative experimental study on sample excitation and probe excitation in force modulation atomic force microscopy. Meas Sci Technol 24:025403.

Yamanaka K, Noguchi A, Tsuji T, Koike T, Goto T. 1999. Quantitative material characterization by ultrasonic AFM. Surf Interface Anal 27:600–606.

Yamanaka K, Ogiso H, Kolosov O. 1994. Ultrasonic force microscopy for nanometer resolution subsurface imaging. Appl Phys Lett 64:178–180.

Zhang L, Dong J. 2012. High-rate tunable ultrasonic force regulated nanomachining lithography with an atomic force microscope. Nanotechnology 23:085303.

Zlatanova J, Lindsay SM, Leuba SH. 2000. Single molecule force spectroscopy in biology using the atomic force microscope. Prog Biophys Mol Bio 74:37–61.